

High Accuracy Mantle Convection Simulation through Modern Numerical Methods

Martin Kronbichler¹

Timo Heister²

Wolfgang Bangerth²

¹ *Department of Information Technology, Uppsala University, Box 337, 751 05 Uppsala, Sweden; martin.kronbichler@it.uu.se*

² *Department of Mathematics, Texas A&M University, College Station, TX 77843-3368; {heister,bangerth}@math.tamu.edu*

30 October 2011

SUMMARY

Numerical simulation of the processes in the Earth mantle is a key piece in understanding its dynamics, composition, history, and interaction with the lithosphere and the earth core. However, doing so presents many practical difficulties related to the numerical methods that can accurately represent these processes at relevant scales. This article presents an overview of the state of the art in algorithms for high-Rayleigh number flows such as those in the earth mantle, and discusses their implementation in the Open Source code ASPECT (Advanced Solver for Problems in Earth's ConvecTion). Specifically, we show how an interconnected set of methods for adaptive mesh refinement (AMR), higher order spatial and temporal discretizations, advection stabilization and efficient linear solvers can provide high accuracy at a numerical cost unachievable with traditional methods, and how these methods can be designed in a way so that they scale to large number of processors on compute clusters.

ASPECT relies on the numerical software packages DEAL.II and TRILINOS, enabling us to focus on high level code and keeping our implementation compact. We present results from validation tests using widely used benchmarks for our code, as well as scaling results from parallel runs.

Key words: Mantle convection, numerical methods, adaptive mesh refinement, finite element method, higher order discretizations, preconditioners

1 INTRODUCTION

Computer simulation has been an important tool in studying the earth mantle owing to its inaccessibility to direct measurements. Consequently, deriving mathematical models and their numerical solution on computers has a long history dating back several decades. Comparing predictions from such models with indirect information about mantle properties (e.g., thermal fluxes, glacial rebound or the shape of the geoid) has provided an enormous amount of insight into the structure and mechanisms driving convection in the mantle. Similar computations have also been used to model other bodies in the solar system.

However, numerical predictions can only be as good as both the mathematical model and the numerical method used to solve it. To this end, more numerical methods have been proposed than we could attempt to summarize here, and a number of well-supported codes implementing the more successful methods have been published under licenses that have allowed their wide usage in the community. Cit-

com [Moresi et al.(1996)] and Conman [King et al.(1990)] are two examples of such codes, and both are now in fact at least in part maintained by the NSF-funded community initiative Computational Infrastructure in Geodynamics (CIG).

While highly successful, both of these codes as well as most others that are in use throughout the community have their roots in numerical methods that were state of the art in the 1980s and early 1990s. For example, they use fixed meshes, low order finite elements, and – measured by today's standards – relatively simple solver and stabilization methods. Acknowledging the difficulty of retrofitting existing codes to new mathematical methods, and with support from CIG, we are therefore implementing a new code for mantle convection from scratch that incorporates the progress that has been made in numerical methods and computational science over the past 20 years. Unlike other efforts that focus on a single part of a simulator (for example the solver, the advection scheme, or the mesh), our intention in this work is to provide a code that uses current technology

in every one of its components. This code, which we call ASPECT (short for *Advanced Solver for Problems in Earth's ConvecTion*) is intended as a modular program that can serve as the basis for both further method development and model refinements, as well as for easy modification to adjust for use in production simulations by the community at large. It is available under an Open Source license.*

In this paper, we summarize the current state of the art in numerical methods and computational science for problems of the kind that appear in the simulation of convection in the earth mantle, and give an overview of the methods implemented in ASPECT. Specifically, we address the following interconnected topics and the strategies used in our code:

- *Mesh adaptation:* Mantle convection problems are characterized by widely disparate length scales (from plate boundaries on the order of kilometers or even smaller, to the scale of the entire earth). Uniform meshes can not resolve the smallest length scale without an intractable number of unknowns. Fully adaptive meshes allow resolving local features of the flow field without the need to refine the mesh globally. Since the location of plumes that require high resolution change and move with time, meshes also need to be adapted every few time steps.

- *Accurate discretizations:* The Boussinesq problem upon which most models for the earth mantle are based has a number of intricacies that make the choice of discretization non-trivial. In particular, the finite elements chosen for velocity and pressure need to satisfy the usual compatibility condition for saddle point problems. This can be worked around using pressure stabilization schemes for low-order discretizations, but high-order methods can yield better accuracy with fewer unknowns and offer more reliability. Equally important is the choice of a stabilization method for the highly advection-dominated temperature equation. We will choose a nonlinear artificial diffusion method for the latter.

- *Efficient linear solvers:* The major obstacle in solving the Boussinesq system is the saddle-point nature of the Stokes equations. Simple linear solvers and preconditioners can not efficiently solve this system in the presence of strong heterogeneities or when the size of the system becomes very large. We will present an efficient solution strategy using a block triangular preconditioner based on an algebraic multi-grid that provides optimal complexity even up to problems with hundreds of millions of unknowns.

- *Parallelization of all of the steps above:* Global mantle convection problems frequently require extremely large

numbers of unknowns for adequate resolution in three dimensional simulations. The only realistic way to solve such problems lies in parallelizing computations over hundreds or thousands of processors. This is made more complicated by the use of dynamically changing meshes, and it needs to take into account that we want to retain the optimal complexity of linear solvers and all other operations in the program.

- *Modularity of the code:* A code that implements all of these methods from *scratch* will be unwieldy, unreadable and unusable as a community resource. To avoid this, we build our implementation on widely used and well tested libraries that can provide researchers interested in extending it with the support of a large user community. Specifically, we use the DEAL.II library [Bangerth et al.(2007), Bangerth & Kansch(2011)] for meshes, finite elements and everything discretization related; the TRILINOS library [Heroux et al.(2005), Heroux et al.(2011)] for scalable and parallel linear algebra; and P4EST [Burstedde et al.(2011)] for distributed, adaptive meshes. As a consequence, our code is freed of the mundane tasks of defining finite element shape functions or dealing with the data structures of linear algebra, can focus on the high-level description of what is supposed to happen, and remains relatively compact at currently only around 1,000 lines. The code will also automatically benefit from improvements to the underlying libraries with their much larger development communities. Our code is extensively documented to enable other researchers to understand, test, use, and extend it.

It is our hope that the code finds adoption in the mantle convection community. This publication is intended as an overview of the numerical methods considered state-of-the-art today and that are implemented in ASPECT.

In the following sections, we will discuss the various parts of developing a modern implementation of a mantle convection simulator. Specifically, in Section 2 we outline the mathematical formulation of the problem in the form of the Boussinesq approximation. Section 3 discusses the numerical methods used for time discretization, spatial discretization and stabilization of the temperature equation, the linear solvers and preconditioners, and parallelization issues. Section 4 shows numerical results obtained with the code and the results of benchmark problems. Section 5 draws conclusions and gives an outlook to further questions.

2 FORMULATION OF THE PROBLEM

Convection processes in the earth's mantle are well described by incompressible fluid flow driven by temperature-induced small density differences. Since viscous friction forces in the fluid are large compared to buoyancy forces, the motion is slow and inertial terms can be neglected [Schubert et al.(2001)]. This yields the Boussinesq model, given by the following set of partial differential equations

$$-\nabla \cdot (2\eta\varepsilon(\mathbf{u})) + \nabla p = \rho(T)\mathbf{g}, \quad (1)$$

$$\nabla \cdot \mathbf{u} = 0, \quad (2)$$

$$\frac{\partial T}{\partial t} + \mathbf{u} \cdot \nabla T - \nabla \cdot (\kappa \nabla T) = \gamma. \quad (3)$$

In this equation, \mathbf{u} denotes the fluid velocity, p the dynamic pressure, and T the temperature. η is the viscosity

* In fact, it isn't at the moment, though we have shared it liberally with others up to this point (and we will be glad to provide anonymous access to the reviewers). We commit to releasing the first public version prior to publication of this paper. What is currently already available is the step-32 tutorial program of deal.II that is the immediate precursor of ASPECT, see http://dealii.org/developer/doxygen/deal.II/step_32.html and that already contains all principal algorithms of ASPECT. The difference between the two codes will primarily be its intent: step-32 is a teaching tool, ASPECT a code aimed at production computations using a modular and extensible design. Release of ASPECT will make this footnote obsolete before final publication.

of the material, and $\varepsilon(\mathbf{u}) = \frac{1}{2}(\nabla\mathbf{u} + (\nabla\mathbf{u})^T)$ is the rate-of-deformation or strain rate tensor. The parameters κ , γ , and \mathbf{g} are the thermal conductivity, heat sources, and gravity vector, respectively. The simplest approximation for the temperature dependent density $\rho(T)$ is to use the relationship

$$\rho(T) = \rho_{\text{ref}}(1 - \beta(T - T_{\text{ref}})),$$

where ρ_{ref} is the reference density at reference temperature T_{ref} , and β is the thermal expansion coefficient. The equations need to be augmented by appropriate boundary conditions for the velocity (or pressure) and temperature, as well as initial conditions for T .

This relatively simple system can be non-dimensionalized by introducing the Rayleigh number, see e.g. [Zhong et al.(2008)] to simplify the analysis of these equations. However, we choose not to do so, since working in the correct physical units makes comparison of numerical results and table lookup of experimentally determined material parameters simpler when using nonlinear and more realistic versions of the equations above. Furthermore, it avoids many easy-to-make programming errors. On the other hand, we will have to pay attention in our linear solvers to avoid the resulting problems with ill-conditioning, a topic we will come back to in Section 3.2.4.

We note that for a realistic description of the earth, several of the coefficients depend on the solution variables. For example, the viscosity η generally decreases with rising temperature T and depends on the strain rate; both viscosity η and density ρ depend on the current location in the p - T phase diagram; and the heating term γ will contain not only radiogenic heating but also adiabatic heating and the viscous dissipation $\eta\varepsilon(\mathbf{u}) : \varepsilon(\mathbf{u})$. Many other factors, for example inhomogeneous chemical composition or phase changes, also enter any attempt at complete descriptions. We will discuss some of these issues at the end of this paper.

3 NUMERICAL METHODS

Equations (1)–(3) are not easy to solve numerically. To be efficient, an algorithm has to take into account a number of interconnected issues related to time stepping, spatial discretization, and linear solvers, none of which can be considered entirely on their own.

As mentioned in the introduction, the purpose of this paper is to describe a coherent set of methods for time discretization, adaptive meshing, spatial discretization, parallelization, and optimal linear solvers and preconditioners that together yield accurate solutions at optimal cost and that enable the numerical simulation even of processes that were previously considered too difficult, or in a fraction of the time for problems that are typically considered expensive.

In the following subsections, we will present the various building blocks of our approach. An open source implementation of these ideas is available through the extensively documented step-31 and step-32 tutorial programs [Kronbichler & Bangerth(2011), Kronbichler et al.(2011)] of the widely used finite element library DEAL.II [Bangerth et al.(2007), Bangerth & Kanschat(2011)], and the continued development of these programs in the form of ASPECT.

The numerical results in Section 4 were obtained with only slightly modified versions of these tutorial programs and are therefore easily replicable. We mention here that the code supports both 2d and 3d computations, obviating the need to develop and debug two separate versions of the methods, and enabling to test the 2d version before switching to production runs in 3d.

3.1 Time discretization

The primary complications of the Boussinesq system (1)–(3) with regard to the time discretization are (i) the nonlinear coupling of all components; and (ii) the fact that the Stokes equations for \mathbf{u}, p do not contain time derivatives and consequently form the equivalent of an algebraic (instantaneous) constraint to the temperature equation that does have a time derivative. The result of these complications are that simple and cheap time marching schemes are not possible. A large number of schemes have been proposed and used over the past decades to approximate solutions to the Boussinesq equations (for recent discussions of methods see [Ismail-Zadeh & Tackley(2010), Gerya(2010)]). However, while appropriate at the time, most of them would not be considered highly accurate or highly efficient by today's standards.

The Stokes equation can be considered as a constraint to the temperature equation that has to hold at any given time in general, and at time steps in particular. Time dependent differential equations of this kind are frequently solved using time stepping methods akin to the IMPES (*implicit pressure explicit saturation*) schemes originally developed for porous media flow simulations [Sheldon et al.(1959), Stone & Garder(1961), Chen(2006)]. In these methods, the variables defined by the constraint are computed from the equations without time derivatives. Here, these are velocities and pressure, and since a linear system needs to be inverted, the step is considered *implicit*. In a second sub-step of the original IMPES scheme, the other variables are then updated using an explicit time step. The IMPES approach allows to decouple the nonlinear Boussinesq system into two simpler, linear subproblems, and therefore leads to an efficient scheme for the solution of the coupled problem.

Since one alternates between the two sub-steps, one can consider them in any order. Let us here first discuss the explicit temperature step and then the implicit Stokes solve. In the following, let t^n denote the time of the n th time step and $k_n = t^n - t^{n-1}$ denote the length of the n th time step. We will then write \mathbf{u}^n, p^n, T^n to indicate approximations of the velocity, pressure and temperature at time t^n .

In order to provide accurate convection dynamics, we approximate the time dependency in the temperature equation (3) using a second-order accurate implicit/explicit time stepping scheme based on the BDF-2 scheme [Hairer & Wanner(1991)]. This scheme is a good compromise between high accuracy (which could be increased using higher order schemes), stability (which typically decreases with the order of the scheme, requiring smaller CFL numbers and consequently higher computational effort), and efficiency of implementation (higher order schemes often become unwieldy as they require complicated initialization during the first few time steps, and require the storage of many solution vectors

from previous time steps). The BDF-2 scheme balances these issues well and leads to reasonable CFL numbers and an accuracy that is balanced with that of the spatial discretization that we will discuss in Section 3.2.

To derive the BDF-2 scheme, we use a quadratic interpolation to find the finite difference approximation of $\frac{\partial T}{\partial t}$ from times t^n, t^{n-1}, t^{n-2} as

$$\frac{\partial T(t^n)}{\partial t} \approx \frac{1}{k_n} \left(\frac{2k_n + k_{n-1}}{k_n + k_{n-1}} T(t^n) - \frac{k_n + k_{n-1}}{k_{n-1}} T(t^{n-1}) + \frac{k_n^2}{k_{n-1}(k_n + k_{n-1})} T(t^{n-2}) \right). \quad (4)$$

Using a Taylor series one can show that this approximation is correct up to second order [Hairer & Wanner(1991)]. The same formulas also hold for $\mathbf{u}(t^n)$, of course. The usual form in which these equations are stated in the literature is obtained by assuming that $k_n = k_{n-1}$, but we want to keep our formulas more general since we need to choose variable time step sizes to satisfy the CFL condition at each time step.

Taking into account the time step sizes k_n and k_{n-1} , we define the linearly extrapolated temperature $T^{*,n}$ as

$$T^{*,n} = \left(1 + \frac{k_n}{k_{n-1}} \right) T^{n-1} - \frac{k_n}{k_{n-1}} T^{n-2}, \quad (5)$$

and similarly for an extrapolated velocity $\mathbf{u}^{*,n}$.

We then arrive at a semi-implicit BDF-2 version of the temperature equation (3) by using $T^{*,n}, \mathbf{u}^{*,n}$ in the advection term, treating the diffusion term implicitly, and using approximation (4) for the time derivative:

$$\begin{aligned} \frac{2k_n + k_{n-1}}{k_n + k_{n-1}} T^n - k_n \nabla \cdot \kappa \nabla T^n &= \frac{k_n + k_{n-1}}{k_{n-1}} T^{n-1} \\ - \frac{k_n^2}{k_{n-1}(k_n + k_{n-1})} T^{n-2} - k_n \mathbf{u}^{*,n} \cdot \nabla T^{*,n} &+ k_n \gamma. \end{aligned} \quad (6)$$

We will discuss solving the discretized version of this equation for T^n in Section 3.3.1. Note that we treat physical heat conduction (diffusion) implicitly while the evaluation of convection and the artificial diffusion terms we will discuss below are made explicit by extrapolation. For a fixed convection this will retain unconditional stability, see [Quarteroni & Valli(1994), p.411]. Since solving the temperature equation does not take more than a few percent of the overall run time of Boussinesq solvers, making diffusion implicit is a useful compromise. Regardless of this detail, the whole scheme is not unconditionally stable, because we extrapolate the convection $\mathbf{u}^{*,n}$ in the temperature equation (6).

The introduction of this explicit convection limits the time step by a Courant-Friedrichs-Lewy (CFL) condition [Quarteroni & Valli(1994)]. Specifically, after spatial discretization (see Section 3.2), the time step k_n must satisfy

$$\text{CFL}_K = \frac{k_n \|\mathbf{u}\|_{\infty, K}}{h_K} \leq C$$

on every cell K , for a constant C that depends on the particular time stepping method as well as the method used for spatial discretization and that is experimentally chosen as large as possible while ensuring that the solution remains stable. Here, h_K is the diameter of cell K , and $\|\mathbf{u}\|_{\infty, K}$ the maximal magnitude of the velocity on K . In our implementation, we have experimentally chosen $C = \frac{1}{5.9p}$ in 2d and

$C = \frac{1}{43.6p}$ in 3d, where p is the polynomial degree with which we discretize the temperature variable, see Section 3.2.5. The difference between 2d and 3d results primarily from the different ratio between edge length and cell diameter h_K as well as from the larger distortion of cells in 3d in the shell geometry we will be using in mantle convection simulations. Note that choosing time steps k_n that satisfy this stability condition necessitates choosing them of variable length as in the formulas above.

We end the discussion of the time discretization with three remarks. First, one might believe that a fully implicit time discretization would allow larger time steps. However, since it is impractical to solve the temperature equation fully coupled with the Stokes equation, our use of the extrapolated velocity \mathbf{u}^* already limits the size of time steps. Furthermore, while fully implicit solutions may be stable for advection problems with a CFL number larger than C , they are typically rather inaccurate with large time steps. Secondly, the BDF-2 scheme requires knowledge of the solution at time instances t^{n-1}, t^{n-2} ; consequently, it can not be used for the very first time step and we initialize the scheme by a single, first-order accurate implicit Euler step. Since most geodynamics applications are not interested in the initial transient phase but the long-term behavior, the reduced accuracy in the initial time step does in general not affect overall results. Finally, after solving for the temperature at time instant t^n using (6), we can compute an updated velocity \mathbf{u}^n using the Stokes system

$$\begin{aligned} -\nabla \cdot (2\eta \varepsilon(\mathbf{u}^n)) + \nabla p^n &= \rho(T^n) \mathbf{g}, \\ \nabla \cdot \mathbf{u}^n &= 0. \end{aligned} \quad (7)$$

Since these equations do not have time derivatives, no special time discretization is necessary here.

3.2 Spatial discretization and stabilization

In each time step, we now first have to solve (6) for the updated temperature T^n , then (7) for the new velocity and pressure. To do so, we need to spatially discretize these equations, for which we use the finite element method.

As with time stepping, spatial discretization raises a number of interconnected issues: (i) What kind of mesh should we choose? (ii) What kind and order of finite elements should we use for the temperature, velocity, and pressure variables? (iii) How can we stabilize the solution of the discrete temperature equation to avoid unphysical oscillations in regions where the temperature has strong gradients? We will discuss these issues in turn in the following.

3.2.1 Choice of meshes and local adaptation

With few and mostly recent exceptions (see, for example, [Burstedde et al.(2008), Stadler et al.(2010), Leng & Zhong(2011), Burstedde et al.(2009), Albers(2000), Davies et al.(2007a), Davies et al.(2007b)]), mantle convection applications have used meshes that are either obtained by uniform refinement of a coarse mesh, or are obtained from a mesh generator. In either case, the mesh is fixed. In contrast, we will here use a mesh that can be dynamically adapted by local adaptive refinement and coarsening of an initial

mesh with a small number of cells. This gives us flexibility to improve mesh resolution close to specific features of the solution, for example strong temperature gradients, and thereby increase the accuracy of the solution. A different view of this adaptive mesh refinement (AMR) technique is that the mesh is a selectively coarsened version of a uniformly refined one where coarsening happens in parts of the volume where the solution is smooth. This notion supports the view that adaptively refined meshes provide about the same overall accuracy as a uniformly refined mesh with the same minimal mesh size, but at a fraction of the numerical cost. Evidence from the more mathematically oriented literature (see, e.g., [Bangerth & Rannacher(2003), Ainsworth & Oden(2000), Babuška & Strouboulis(2001)]) shows consistently that AMR can achieve levels of accuracy typically required in engineering applications with a factor of around 100 (in 2d) or 1000 (in 3d) less computational effort than uniformly refined meshes. Convection problems are certainly a prime candidate for savings of this order of magnitude given that the temperature and accompanying flow features frequently vary on length scales of only a few kilometers, much smaller than the size of Earth as a whole. Using adaptively refined meshes is, therefore, a crucially important factor in making highly accurate simulations of complex problems possible at all.

There are a number of practical aspects to using AMR. First, the underlying software is unsurprisingly much more complex than when one wants to use a fixed mesh. Our work is based on a large finite element library, DEAL.II, that already provides this functionality at little additional effort to the implementer of a code, for quadrilaterals in 2d and hexahedra in 3d. Secondly, one has to deal with the fact that if neighboring cells differ in refinement level, some of the nodes of the mesh lie on the midpoints of edges or faces of neighboring cells. We deal with this through constraints that ensure that the solution remains continuous at these *hanging nodes*, see [Babuška & Rheinboldt(1978), Carey(1997), Bangerth et al.(2007), Bangerth & Kayser-Herold(2009)]. Finally, we dynamically adapt the mesh every few time steps and we need a criterion to decide which cells to refine or coarsen. Since the variable that is most indicative of abruptly changing features of the solution is the temperature, we apply a criterion to the temperature that is commonly referred to as the “Kelly error indicator” [Gago et al.(1983)] and that computes for each cell an approximation of the size of the second derivatives times the diameter of the cell. This criterion has been found to be a simple, yet universally useful tool in adaptively refining meshes, and is implemented in DEAL.II. While this works well in 2d, in 3d it refines primarily into the boundary layers at the inner and outer margins of the mantle; we avoid this by also taking derivatives of the velocity into account when refining. Even though we adapt the mesh every few time steps, we limit the number of times a single coarse mesh cell can be refined: otherwise, close to steep gradients, the cells would be made smaller and smaller in each refinement step, requiring smaller and smaller global time steps due to the CFL condition.

While implementing the data structures and algorithms outlined above from scratch would require several tens of thousands of lines of codes, they are all readily available in DEAL.II. In fact, using adaptive meshes and related algorithms requires little more than maybe a dozen lines of code

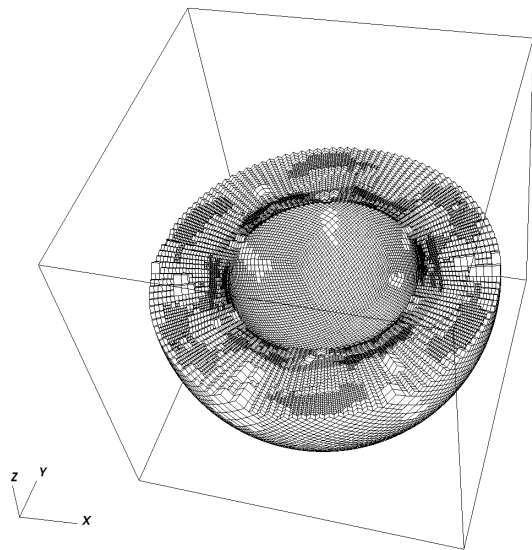


Figure 1. Example of a locally refined mesh. One half of the mesh for the spherical shell geometry in 3d is shown. The mesh has approximately 890,000 cells; the finest cells are six times refined from the coarse mesh.

in our program. An example of the kind of meshes we use here is shown in Fig. 1 in 3d; a 2d mesh is shown in Fig. 5 below.

3.2.2 Approximation of geometry

Our program uses Cartesian coordinates. The advantage of this choice is that the shell geometry of the earth mantle is not a hard-coded special case, but no different than any other geometry (it is simply produced by using a mesh consisting of an unstructured collection of coarse cells which are then hierarchically refined) and the code can readily be adapted to use a box geometry (as used in some of the examples in Section 4), an octant of the shell, or a domain that takes into account the geoid shape or actual topography – none of these is any more difficult than any other, and we need not modify the assembly of matrices or vectors when changing between coordinate systems.

To deal with curved boundaries, one has to map the finite element shape functions discussed below from the reference cell on which they are defined to the location of cells in the unstructured mesh. Traditionally, this is done using polynomial mappings, often chosen to be isoparametric, i.e., of the same polynomial degree as the shape functions [Brenner & Scott(2002), Carey(1997)], though DEAL.II allows these to be chosen independently. Because the overhead of using a higher order mapping is negligible compared to the many other operations in a program (the higher order mapping only leads to higher numerical cost in cells at the surface of the domain), we use a mapping of degree four.

3.2.3 Spatial approximation of the flow variables

On the meshes as described above, we discretize all variables using the finite element method, i.e., we seek to find

approximations for \mathbf{u}^n, p^n, T^n of the form

$$\begin{aligned} \mathbf{u}_h^n(\mathbf{x}) &= \sum_{j=1}^{N_u} U_j^n \boldsymbol{\varphi}_j^u(\mathbf{x}), \\ p_h^n(\mathbf{x}) &= \sum_{j=1}^{N_p} P_j^n \varphi_j^p(\mathbf{x}), \\ T_h^n(\mathbf{x}) &= \sum_{j=1}^{N_T} T_j^n \varphi_j^T(\mathbf{x}). \end{aligned} \quad (8)$$

There are a number of choices for the finite element basis functions $\boldsymbol{\varphi}_j^u, \varphi_j^p, \varphi_j^T$. Since we will want to match the polynomial degree of the functions for the temperature to those of the velocity, let us here first discuss the choice for the flow variables.

For the Stokes system (7), it is well known that the polynomial degrees of shape functions for the velocity and the pressure can not be chosen arbitrarily (see, for example, [Brenner & Scott(2002), Braess(1997)]). Rather, one either has to stabilize the Stokes equations, for example by adding an artificial compressibility term, or by choosing a pair of finite element spaces that satisfy the Babuška-Brezzi (or LBB or inf-sup) condition.

Most homegrown codes use artificial compressibility (or some other) stabilization because it avoids the need to implement shape functions of different polynomial degrees. However, it is known that the resulting solutions are not very accurate; furthermore, these schemes can not easily guarantee mass conservation. For these reasons, we choose to use finite element spaces that are known to be LBB-stable [Girault & Raviart(1986)]. Specifically, we consider the following two options that are already implemented in DEAL.II:

- $Q_{q+1}^d \times Q_q$, ($q \geq 1$): This choice uses continuous shape functions of polynomial degree $q+1$ for each of the d velocity components, and continuous shape functions of polynomial degree q for the pressure.[†] This combination is known as Taylor-Hood elements. The fact that we use a lower polynomial degree for the pressure is not usually a concern since one is not typically interested in highly accurate pressure fields anyway. Furthermore, the pressure is a globally smooth function and almost entirely dominated by the hydrostatic pressure that essentially determines the lookup of pressure-dependent material properties.

- $Q_{q+1}^d \times P_{-q}$, ($q \geq 1$): This choice differs from the one above in that it uses *discontinuous* elements of polynomial degree q for the pressure and that it omits the tensor product shape functions from the polynomial space.

In either case, one will typically choose $q = 1$, i.e., linear

[†] Here and in the following, the finite element space Q_q is generated by mapping *complete tensor polynomial* spaces from the reference cell to each cell. For example, in 2d the space Q_1 consists of the *bilinear* functions $1, \xi, \eta, \xi\eta$, where ξ, η are the coordinates on the reference cell. In contrast, the space P_q consists only of polynomials of *maximum* degree q . In 2d, P_1 consists of the functions $1, \xi, \eta$. Using a negative index, P_{-q} , indicates that functions do not need to be continuous across cell interfaces. See also [Elman et al.(2005), Sec. 5.3] for a discussion of element spaces suitable for the Stokes problem.

elements for the pressure and quadratic ones for the velocity. This gives formal third order accuracy for the velocity variable and second order for the pressure. Choosing larger values for q , as is possible through ASPECT's input file, would yield higher orders of convergence, but non-smooth regions in the solution usually limit the global accuracy so that the additional work does not pay off.

Which of the two choices above for the pressure space is preferable is not immediately obvious. It is easy to show that the second implies local mass conservation on each cell, i.e., $\int_{\partial K} \mathbf{n} \cdot \mathbf{u}_h^n = 0$ for every cell K of the mesh. On the other hand, this does not necessarily yield a smaller overall error and, in fact, simple experiments show that the *pointwise* values of the divergence of \mathbf{u}_h^n are in fact larger for the second choice than for the first. A different consideration is that the second choice has significantly more pressure variables than the first although as we will see in Section 3.3.2, this does not result in a significantly higher computational effort. To facilitate experiments, our implementation allows to choose either based on a run-time parameter.

3.2.4 Weak form and fully discrete Stokes system

The coefficients U_j, P_j of the expansion (8) are determined by inserting \mathbf{u}_h^n, p_h^n into the Stokes system (7), multiplying the equations with test functions $\boldsymbol{\varphi}_i^u(\mathbf{x}), \varphi_l^p(\mathbf{x})$ respectively, and integrating over the domain. Integrating these terms by parts and using the appropriate boundary conditions on $\boldsymbol{\varphi}_i^u$ and \mathbf{u}_h^n then yields the weak form of the discrete equations:

$$\begin{aligned} (\varepsilon(\boldsymbol{\varphi}_i^u), 2\eta\varepsilon(\mathbf{u}_h^n))_\Omega - (\nabla \cdot \boldsymbol{\varphi}_i^u, p_h^n)_\Omega &= (\boldsymbol{\varphi}_i^u, \rho(T_h^n)\mathbf{g})_\Omega, \\ (\varphi_l^p, \nabla \cdot \mathbf{u}_h^n)_\Omega &= 0. \end{aligned}$$

Our goal is to find functions \mathbf{u}_h^n and p_h^n – i.e., to find coefficients U_j, P_j – such that these equations hold for $i = 1 \dots N_u, l = 1 \dots N_p$. As stated, the equations are unbalanced in their physical units since we have not non-dimensionalized them, and will have vastly different numerical values when using coefficients and length scales as common for Earth. While not a mathematical problem, it leads to severe inaccuracies for both linear and iterative solvers. We avoid these by multiplying the second of the two equations by a pressure scaling factor $s_p = \frac{\eta}{L}$ where L is a typical lengthscale of the problem. We have found that it is best to choose L not as the diameter of the domain but as the size of typical features such as plumes in the earth to approximate the effect of the missing second derivative in the second equation compared to the first. For example, for global convection problems, we choose $L = 10^4$ m.

After multiplying the second equation by s_p , the system is no longer symmetric. We can restore symmetry by replacing the pressure by $p_h^n = s_p \bar{p}_h^n$ and solving for \bar{p}_h^n with expansion coefficients \bar{P} instead. We obtain the original pressure immediately after solving by multiplying the pressure component of the solution vector by s_p . With all this, the fully discrete version of the Stokes equations at time step n now reads

$$\begin{aligned} (\varepsilon(\boldsymbol{\varphi}_i^u), 2\eta\varepsilon(\mathbf{u}_h^n))_\Omega - s_p (\nabla \cdot \boldsymbol{\varphi}_i^u, \bar{p}_h^n)_\Omega &= (\boldsymbol{\varphi}_i^u, \rho(T_h^n)\mathbf{g})_\Omega, \\ s_p (\varphi_l^p, \nabla \cdot \mathbf{u}_h^n)_\Omega &= 0, \end{aligned} \quad (9)$$

and we can rewrite these equations in matrix notation as

$$\begin{pmatrix} A & B^\top \\ B & 0 \end{pmatrix} \begin{pmatrix} \mathbf{U}^n \\ \bar{\mathbf{P}}^n \end{pmatrix} = \begin{pmatrix} \mathbf{F}^n \\ 0 \end{pmatrix}, \quad (10)$$

where

$$A_{ij} = (\varepsilon(\varphi_i^u), 2\eta\varepsilon(\varphi_j^u))_\Omega, \quad (11)$$

$$B_{ij} = -s_p(\varphi_i^q, \nabla \cdot \varphi_j^u)_\Omega, \quad (12)$$

$$F_i = (\varphi_i^u, \rho(T)\mathbf{g})_\Omega \quad (13)$$

with right-hand side vector F . We will discuss solving this linear system in Section 3.3.2.

3.2.5 Spatial approximation of the temperature variable

Since the temperature structure of the earth is one of the variables of primary interest in mantle convection computations, we are interested in an accurate representation. Consequently, choosing a higher order approximation would seem promising. On the other hand, we can not expect the evolution of the temperature field to be more accurate than the velocity field along which it is primarily advected. Thus, we choose to approximate the temperature using the same polynomial degree $q + 1$ as the velocity, i.e., $T_h^n \in Q_{q+1}$. Our experience is that Q_q elements yield considerably worse approximations in usual temperature fields, despite the fact that high order methods are more prone to over- and undershoots in regions of high gradients [LeVeque(2002)]. We suppress these oscillations through an appropriate stabilization as discussed in the next section.

3.2.6 Stabilization of the temperature equation

Equation (6) for the temperature at time step n is of advection-diffusion type. In mantle convection simulations, the diffusivity κ is very small compared to the velocity. Even for very fine meshes, the local Péclet number on cell K , $\text{Pe}_K = \frac{h_K|\mathbf{u}|_K}{\kappa}$ is usually in the range of 10^2 to 10^4 . For such high Péclet number problems, standard finite element discretizations introduce spurious oscillations around steep gradients [Donea & Huerta(2003)]. Therefore, stabilization must be added to the discrete formulation in order to obtain correct solutions.

One commonly used stabilization is to add artificial diffusion, either uniformly or, in the SUPG method, only along streamlines [Brooks & Hughes(1982)]. Such methods are used, for example, in the widely used Conman [King et al.(1990)] and Citcom [Moresi et al.(1996)] codes. While popular, these methods have the disadvantage that they add diffusion everywhere, even in regions where the temperature is smooth and there is no danger of oscillations. We therefore adopt a more recent method, the so-called entropy viscosity method [Guermont et al.(2011)], that only adds artificial diffusion where necessary. This method solves the modified temperature equation

$$\frac{\partial T}{\partial t} + \mathbf{u} \cdot \nabla T - \nabla \cdot (\kappa + \nu_h(T))\nabla T = \gamma, \quad (14)$$

subject to the time discretization discussed in Section 3.1, with an artificial dissipation $\nu_h(T)$ added to the equation. Conceptually, in regions where the temperature field T is smooth ν_h should be small, and in regions with significant variability ν_h should be of similar size as the diffusive flux in a first order upwind scheme [LeVeque(2002)]. This nonlinear definition of the artificial viscosity makes sure that the dissipation is as small as possible, while still large enough to

prevent oscillations in the temperature field. In particular, the global approximation property of the scheme will not be affected, as would be with a simple linear dissipation with a constant ν_h .

Following [Guermont et al.(2011)], on cell K we choose $\nu_h|_K$ as

$$\nu_h|_K = \min(\nu_h^{\max}|_K, \nu_h^E|_K). \quad (15)$$

The maximum dissipation ν_{\max} is defined as

$$\nu_h^{\max}|_K = \alpha_{\max} h_K \|\mathbf{u}\|_{\infty, K},$$

where the constant $\alpha_{\max} = 0.026d$ depends only on the spatial dimension d , and where h_K denotes the characteristic size of cell K . On the other hand, the entropy viscosity is defined as

$$\nu_h^E|_K = \alpha_E \frac{h_K^2 \|r_E(T)\|_{\infty, K}}{\|E(T) - E_{\text{avg}}\|_{\infty, \Omega}},$$

where we choose the constant $\alpha_E = 1$, see also the discussion in [Guermont et al.(2011)]. The entropy viscosity is scaled globally by $\|E(T) - E_{\text{avg}}\|_{\infty, \Omega}$, based on the maximum deviation of the temperature entropy $E(T) = \frac{1}{2}(T - T_m)^2$, $T_m = \frac{1}{2}(T_{\min} + T_{\max})$ from the space-average $E_{\text{avg}} = \frac{1}{|\Omega|} \int_\Omega E(T)$. The residual $r_E(T)$ is associated with the entropy of the temperature equation,

$$r_E(T) = \frac{\partial E(T)}{\partial t} + (T - T_m) (\mathbf{u} \cdot \nabla T - \kappa \nabla^2 T - \gamma).$$

This residual is zero if applied to the exact solution of the temperature equation, leading to no artificial diffusion, but it is nonzero when applied to the numerical approximation we compute and will be large in areas where the numerical approximation is poor, such as close to strong gradients. We note that this definition of an artificial dissipation is similar to the YZ β discontinuity capturing proposed in [Bazilevs et al.(2007)], where the residual is based on the equation itself instead of the entropy, though.

In practice, we need to evaluate the formula above for the discrete solution. Since we do not want the artificial viscosity to introduce a nonlinear dependence on the current temperature T^n , we make it explicit by approximating the time derivative from the two previous time levels in the BDF-2 time stepping, $\partial E(T^h)/\partial t \approx (E(T^{n-1}) - E(T^{n-2}))/k_{n-1}$, and evaluating all other occurrences of the temperature at the midpoint as $(T^{n-1} + T^{n-2})/2$, including the average temperature. We will treat the artificial viscosity term $-\nabla \cdot \nu_h(T^{n-1}, T^{n-2})\nabla T^{*,n}$ as a whole explicitly, based on the extrapolated temperature defined in (5). Since the maximum artificial viscosity is proportional to the mesh size and the velocity, the CFL number is not changed substantially, which we have also verified numerically.

3.2.7 Fully discrete temperature system

In the same way as for the Stokes equations, we obtain the fully discrete linear system corresponding to the time-discretized temperature equation (6):

$$\left(\frac{2k_n + k_{n-1}}{k_n + k_{n-1}} M + k_n K \right) T^n = G^n, \quad (16)$$

where $M_{ij} = (\varphi_i^T, \varphi_j^T)_\Omega$ is the mass matrix, and $K_{ij} = (\kappa \nabla \varphi_i^T, \nabla \varphi_j^T)_\Omega$ the stiffness matrix. The right hand side

term G^n contains all terms from previous time levels,

$$G_i^n = \left(\varphi_i^T, \frac{k_n + k_{n-1}}{k_{n-1}} T^{n-1} - \frac{k_n^2}{k_{n-1}(k_n + k_{n-1})} T^{n-2} \right)_\Omega \\ + \left(\varphi_i^T, -k_n \mathbf{u}^{*,n} \cdot \nabla T^{*,n} + k_n \gamma \right)_\Omega - \left(\nabla \varphi_i^T, k_n \nu_h \nabla T^{*,n} \right)_\Omega,$$

where the artificial viscosity ν_h is defined by (15) and constant within a cell K , and the extrapolated values for temperature and velocity are according to (5).

3.3 Linear solvers

Applying temporal and spatial discretization to the Boussinesq system leads to the two linear equation systems (16) and (10) that need to be solved in each time step. To accurately represent problems in geodynamics, this leads to large systems with up to hundreds of millions or billions of unknowns for which the only realistic choice are iterative solvers [Saad(2003)]. We discuss our choices in the following sections.

3.3.1 Temperature system

Solving the temperature system (16) is relatively straightforward. The system is symmetric, positive definite, and dominated by the mass matrix part since the remainder is proportional to $k_n \kappa = \frac{h^2}{\text{Pe}}$ with typical local Péclet numbers on the order of 100 or more. Consequently, the eigenvalues of the matrix are well clustered, independent of the mesh size, and the CG method converges in a number of steps independent of the mesh size [Saad(2003)]. We use an incomplete LU decomposition as a preconditioner. Typical iteration counts are between 10 and 30.

3.3.2 Stokes system

The Stokes system (10) is more challenging because of the saddle point structure with zero diagonal block. Solving linear equations with such a structure is discussed in great detail in [Elman et al.(2005)]. An extensive overview of methods for the Stokes system in the context of mantle convection is given in [Geenen et al.(2009)], and we basically follow their approach.

Of the available iterative solvers for indefinite symmetric problems such as GMRES, SymmLQ or MinRes [Saad(2003)], only GMRES can deal with the non-symmetric preconditioners we will discuss below and that have been shown to be the most efficient for this problem. Standard GMRES determines whether to stop the iteration by estimating the norm of the residual based on preconditioned iterates. Since the preconditioner we consider below uses inexact solves, it is not a linear operation, and consequently the residual estimate is inaccurate and not a reliable stopping criterion. Therefore, we use the flexible GMRES (FGMRES) variant of GMRES that uses one explicit residual computation per iteration to determine whether the stopping criterion has been met.

Any iterative solver for large problems requires preconditioners to lower the condition number of linear systems, preferably to a value that is independent of the mesh size. This could in principle be done by looking at the matrix as

a whole (see, for example, [Saad(2003)], or the multigrid approach in [Kameyama(2005)]), but is uncommon for block systems such as the one considered here. Rather, most efficient preconditioners found so far for the Stokes system are based on variants of the ones described in [Silvester & Wathen(1994)] and are defined by the non-symmetric block triangular matrix

$$P = \begin{pmatrix} A & B^\top \\ 0 & -S \end{pmatrix}, \quad \text{with} \quad P^{-1} = \begin{pmatrix} A^{-1} & A^{-1} B^\top S^{-1} \\ 0 & -S^{-1} \end{pmatrix}$$

where $S = BA^{-1}B^\top$ is the Schur complement of the Stokes operator. Applying P^{-1} as a right preconditioner yields

$$\begin{pmatrix} A & B^\top \\ B & 0 \end{pmatrix} P^{-1} = \begin{pmatrix} I & 0 \\ BA^{-1} & I \end{pmatrix},$$

for which it can be shown that GMRES converges in at most two iterations [Silvester & Wathen(1994)].

This preconditioner is not practically useful because it involves exact inverses A^{-1} and S^{-1} . In our computations, we therefore use the following preconditioner instead:

$$P^{-1} = \begin{pmatrix} \widetilde{A}^{-1} & -\widetilde{A}^{-1} B^\top \widetilde{S}^{-1} \\ 0 & \widetilde{S}^{-1} \end{pmatrix} \quad (17)$$

where $\widetilde{A}^{-1}, \widetilde{S}^{-1}$ approximate the exact inverses. We will discuss our choices for these matrices next. In their construction, it is important to remember that iterative solvers do not need element-by-element representations of matrices like \widetilde{A}^{-1} but only the results of products like $\widetilde{A}^{-1}r$ for a given vector r , whichever way this can be computed.

Choice of \widetilde{A}^{-1} . Since A is symmetric, we compute the product $x = \widetilde{A}^{-1}r$ by solving the linear system $Ax = r$ for x using a CG solver with a loose tolerance of 10^{-2} (relative residual). This is a sufficient approximation, and the outer GMRES solver will take care that the solution to the whole system will converge to the desired tolerance.

This approximate CG solve needs to be preconditioned. Candidate preconditioners that yield mesh-independent convergence are multigrid methods, see e.g. [Hackbusch(1985), Trottenberg et al.(2001)]. We use the algebraic multigrid (AMG) implementation provided as part of the ML package [Tuminaro & Tong(2000), Gee et al.(2006)] of the TRILINOS library [Heroux et al.(2005), Heroux et al.(2011)] for this purpose due to its robustness with respect to variable viscosities and scalability even on very large parallel machines.

The performance of the ML-AMG preconditioner depends on the sparsity structure of the matrix. High order methods and systems where the different vector components of shape functions couple like in the A matrix in (11) tend to deteriorate the quality of the preconditioner, see also [Geenen et al.(2009)]. Therefore, when preconditioning the inexact solution of A , we do not apply the AMG to the A matrix but instead to a matrix \hat{A} with

$$\hat{A}_{ij} = \sum_{d=1}^{\dim} (\varepsilon([\varphi_i^u]_d \mathbf{e}_d), 2\eta \varepsilon([\varphi_j^u]_d \mathbf{e}_d))_\Omega \\ = (\nabla \varphi_i^u, 2\eta \nabla \varphi_j^u)_\Omega,$$

where \mathbf{e}_d is the unit vector in coordinate direction d . In other words, the bilinear form that defines \hat{A} does not couple shape functions that correspond to different velocity components, and \hat{A} consequently has only one third of the number of entries as A in three space dimensions. On the other hand, we

note that when building this preconditioner matrix, we have to ensure that it respects the correct set of boundary conditions on the velocity which may introduce coupling between vector components after all if the boundary conditions require tangential flow; forgetting this coupling turns out to have a devastating effect on the quality of the preconditioner.

Choice of \widetilde{S}^{-1} . The inverse of the Schur complement matrix $S = BA^{-1}B^T$ can be accurately approximated by the inverse of a (weighted) mass matrix in pressure space with entries $M_{ij}^p = (\eta^{-1}\varphi_i, \varphi_j)$. This can be explained by the fact that B approximates a gradient operator, B^T a divergence operator, whereas A^{-1} is the inverse of a matrix that is spectrally close to a Laplace matrix, see also [Silvester & Wathen(1994)].

Consequently, we choose $\widetilde{S}^{-1} = (M^p)^{-1}$ in the preconditioner, and computing the action $\widetilde{S}^{-1}r$ on a vector r only requires an approximate CG solve with M^p , which we precondition using an ILU of M^p . This solver converges in 1–5 iterations. This is again independent of the mesh size since the condition number of the mass matrix is independent of the refinement level.

Compared to the application of \widetilde{A}^{-1} , this step is cheap. Consequently, choosing the larger but locally conservative pressure space P_{-q} over the smaller space Q_q (see Section 3.2.3) has only a minor effect on overall run times; furthermore, the matrix M^p is block diagonal when using the discontinuous space P_{-q} , making the inversion of this matrix particularly cheap.

Summary of preconditioner. In summary, applying the preconditioner (17) to a vector, i.e., computing

$$\begin{pmatrix} x_U \\ x_P \end{pmatrix} = P^{-1} \begin{pmatrix} r_U \\ r_P \end{pmatrix}$$

requires the following steps:

- form $x_P = \widetilde{S}^{-1}r_P$ by performing an inexact CG solve with ILU preconditioner of the system $M^p x_P = -r_P$;
- compute $y = r_U - B^T x_P$
- form $x_P = \widetilde{A}^{-1}y$ by performing an inexact CG solve of the system $Ax_U = y$ with ML-AMG preconditioner based on the matrix \hat{A} .

Overall performance of solver. The components of the linear solvers outlined above are chosen in such a way that they provide a performance that is mostly mesh size independent and can therefore scale from small to very large problems. In particular, in accordance with theoretical considerations, we observe that the number of outer FGMRES iterations is independent of the mesh size, whereas the number of iterations in the inner solves with the velocity block using the AMG preconditioner increases only weakly (for example, from 10 to 15 iterations when increasing the number of unknowns from 10^6 to $2.4 \cdot 10^8$). Inversion of the pressure mass matrix also requires a number of iterations that is independent of the mesh size. The total number of operations for solving the linear Stokes system is therefore almost linear in the number of unknowns, and thus of almost optimal complexity. We verify this through weak scaling experiments in Section 4.3.

It is possible that the solver performance can be further improved by noting that there is a tradeoff between the

accuracy in inverting \hat{A} and the number of outer FGMRES iterations. For example, one could choose \widetilde{A}^{-1} to be only a single, cheap V-cycle with \hat{A} at the expense of more outer iterations (see also [Geenen et al.(2009)]). On the other hand, while overall faster for isoviscous problems, we observe that this occasionally leads to a breakdown of the iteration and is therefore not robust. Consequently, we are experimenting with first trying a preconditioner that only employs a single V-cycle and, if FGMRES has not converged in a certain number iterations with this preconditioner, switching to the more accurate preconditioner that actually uses the approximate inverse of A . We will report on results for this scheme elsewhere.

We end this section by noting that the number of FGMRES iterations can be reduced by more than a factor of 5 (from an average of around 40 to an average around 7) by not starting the iteration with a zero vector, but rather with the extrapolation of the solution vector from the previous time steps using a formula like (5), providing a very significant speedup of the overall runtime.

3.4 Parallelization

The simulation of three-dimensional mantle convection requires highly resolved computations, with sometimes hundreds of millions or billions of unknowns, in order to yield reliable results. With today's computer hardware, these requirements cannot be met on single machines, but instead needs parallelization, see also [Burstedde et al.(2008)]. Our implementation of the algorithms outlined above provides for parallelization both via MPI between a possibly large number of distributed memory machines as well as via threads on shared memory machines or within individual nodes of a cluster of computers. Both kinds of parallelization are mostly transparent to the application code and are primarily handled in library code in DEAL.II (for the mesh and finite element specific parts) or TRILINOS (for the linear algebra).

To be efficient, parallelization requires that *all* parts of a program be parallelized to the same degree. In adaptive finite element codes, this implies that the mesh creation, assembly of linear systems, linear solvers and preconditioners, postprocessing steps such as the evaluation of the solution, generation of output files for visualization, or the evaluation of error indicators, and the adaptation of the mesh are all parallelized. Our code provides for all of these components. In particular, all mesh operations in DEAL.II build on the P4EST library for parallel mesh management [Burstedde et al.(2011)] that has been shown to scale to more than 200,000 processors, and the linear algebra components in TRILINOS's Epetra and ML packages have also been demonstrated to scale to machines of this size. We have previously verified the scalability of a large number of DEAL.II components up to at least 16,384 processor cores in [Bangerth et al.(2011)] where we also report on scalability of a 2d version of the code discussed here. We show additional data below in Section 4.3.

4 RESULTS

To verify the correctness, accuracy and efficiency of our code, we have run a number of convection benchmarks. We report results on two of these below, namely one of the 2d benchmarks from [Blankenbach et al.(1989)] in Section 4.1 and one of the 3d benchmarks from [Busse et al.(1993)] in Section 4.2, both of which are widely used in other papers as well. We show parallel scalability in Section 4.3 and some results of global mantle convection simulations in Section 4.4.

Additional parallel scalability analyses are provided in [Bangerth et al.(2011)] and we will report on results for the semi-analytic benchmark of [Tan & Gurnis(2007)] in [Geenen et al.(2011)], where we also demonstrate that convergence rates match theoretical expectations, in addition to the overall accuracy levels reported here.

4.1 2d benchmark problem

We compare our implementation to the well-known two-dimensional dynamic benchmark problem described in [Blankenbach et al.(1989)]. The benchmark is solved in non-dimensional units in the form of equation (1)–(3), using the parameters given in Table 1. The computational domain is the rectangle $[0, l] \times [0, h]$. The strength of buoyancy is described by the Rayleigh number $Ra = \beta g \gamma h^5 / \kappa^2 \rho c_p \eta = 216,000$. The body is heated homogeneously from within with a non-dimensional heat rate $\gamma = 1$.

On the side boundaries, reflective symmetry conditions are assumed, i.e., no-normal-flux for velocity, $\mathbf{u} \cdot \mathbf{n} = 0$ and $\mathbf{n} \cdot \nabla T = 0$. On the top and bottom, no-slip conditions $\mathbf{u} = 0$ are applied. On the bottom face, the temperature flux is zero, $\mathbf{n} \cdot \nabla T = 0$, and we set $T = 0$ on the top face. The simulation is started with a perturbation from the purely conductive state and is run until we reach the periodic cycle after around non-dimensional time $t = 2$. A snapshot of the solution is shown in Fig. 2 (top).

We compare results using two measures: (i) the Nusselt number, defined as the ratio between the mean surface temperature gradient and the mean bottom temperature,

$$\text{Nu} = - \frac{\int_{\partial\Omega_t} \nabla T \cdot \mathbf{n} \, ds}{\int_{\partial\Omega_b} T \, ds}, \quad (18)$$

where $\partial\Omega_t$ is the top face at $z = h$ and $\partial\Omega_b$ the bottom face at $z = 0$. And (ii) the (non-dimensional) root mean square velocity

$$v_{\text{rms}} = \sqrt{\frac{1}{hl} \int_{\Omega} |\mathbf{u}|^2 \, dx}. \quad (19)$$

The bottom panel of Fig. 2 shows a phase diagram with the Nusselt number over the rms velocity, illustrating the periodic nature of the flow after the initial transient has decayed.

We compare the values we obtain for the two measures above to the benchmark data in [Blankenbach et al.(1989)]. The results for different mesh sizes with global (non-adaptive) mesh refinement are given in Table 2, and results with adaptive mesh refinement are given in Table 3. These results show that we correctly reproduce the benchmark

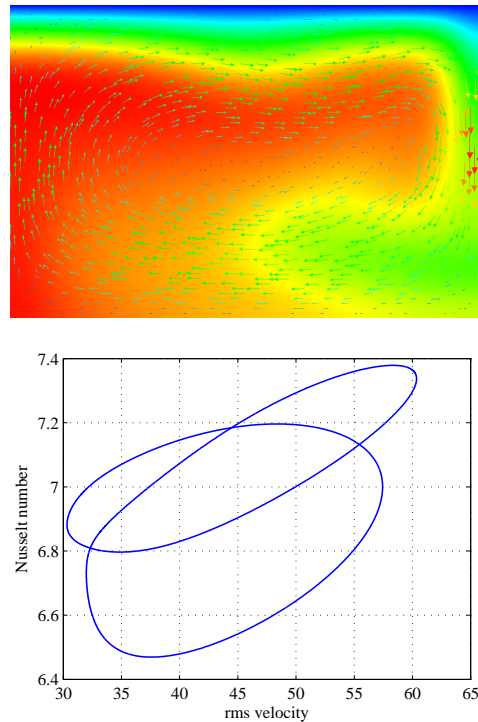


Figure 2. 2d benchmark. Top: Temperature field (with values between 0 and 0.1793) and velocity field (with velocities up to 89.4) for one time step. Bottom: Nusselt number over rms velocity. The curve shows the time evolution after the initial transient has decayed and illustrates the periodic nature of the flow.

results and the substantial savings that can be obtained through adaptive meshes. Not surprisingly, given the advances in numerical methods and computer hardware since [Blankenbach et al.(1989)], we believe that our results are substantially more accurate than the ones given in the original reference.

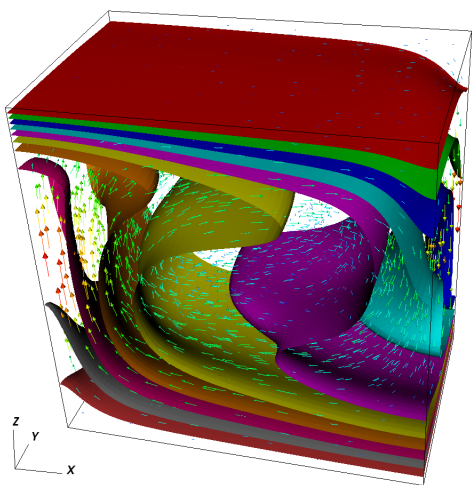
4.2 3d benchmark problem

As a three-dimensional benchmark, we choose benchmark problem 1a from [Busse et al.(1993)]. The problem is posed in a box of dimensions $a \times b \times 1$ with $a = 1.0079$ and $b = 0.6283$, and for Rayleigh number $Ra = 30,000$. The flow develops to a stationary bimodal flow. A snapshot is shown in Fig. 3.

To find the steady state, we simulate the problem up to non-dimensional time $t = 5$ and record values for the Nusselt number (18) and root mean square velocity (19). Moreover, we also compare the average temperature T_m over the plane $z = 0.75$, point values for the vertical velocity u_3 and temperature at $(0, 0, 0.5)$, and the heat flux $Q(x_1, x_2) = \frac{\partial T}{\partial x_3}|_{x_3=1}$ at the top surface. Results for mesh sizes $24 \times 14 \times 24$, $32 \times 20 \times 32$ and $48 \times 30 \times 48$ (with approximately 220k, 540k and 1.8M unknowns for the velocity/pressure system and 70k, 170k and 570k temperature unknowns) are recorded in Table 4. The results are in good accordance with the reference values, which shows correctness of our implementation also in three spatial dimensions. Note that quantities derived from the FE function values (v_{rms} , T , u_3) are considerably more accurate for

Table 1. Parameters for the benchmark discussed in Section 4.1 based on [Blankenbach et al.(1989)].

	Explanation	Nondim. value	Dim. value (SI-units)
h	Cell height	1	10^6
l	Cell length	1.5	$1.5 \cdot 10^6$
ρ	Fluid density	1	$4 \cdot 10^3$
η	Kinematic viscosity	1	$1.157 \cdot 10^{18}$
κ	Thermal diffusion	1	10^{-6}
g	Gravity acceleration	1	10
β	Thermal expansion coefficient	1	$2.5 \cdot 10^{-5}$
γ	Rate of internal heating	1	$5 \cdot 10^{-9}$
c_p	Heat capacity	1	$1.25 \cdot 10^3$
Ra	Rayleigh number	$2.16 \cdot 10^5$	—


Figure 3. 3d benchmark. Velocity field and isosurfaces of the temperature.

coarser meshes than those derived from gradients (Nu , Q). On current hardware and running without parallelization, each time step takes on average approximately 2.5s, 6s, 15s for the three different meshes, respectively.

4.3 Scalability of the solution scheme

Having verified the correctness of the solver, let us now consider its scalability and efficiency. To this end, we start with a spherical shell consisting of 96 coarse mesh cells which we refine either adaptively or globally a number of times until we reach a desired number of unknowns. On this mesh, we then perform one complete time step of our scheme and measure the wall time for the major building blocks of our code for a fixed number of MPI processes each tied to one CPU core (weak scaling). Alternatively, we select a fixed mesh size and measure times for a variable number of MPI processes (strong scaling). Specifically, we measure the run time of the following components:

- *Setup DoFs*: This includes giving all degrees of freedom globally unique numbers, computing constraints for hanging nodes, evaluating boundary values, and setting up matrices and vectors.

- *Assemble Stokes*: Computing and assembling the entries of the Stokes matrix and right hand side.
- *Build preconditioner*: Computing and assembling the entries for the Stokes preconditioner matrices as well as initializing the AMG preconditioner for \hat{A} .
- *Solve Stokes*: Solving the Stokes system.
- *Assemble T RHS*: Computing and assembling the entries of the right-hand side vector for the temperature system.
- *Solve T*: Solving the temperature equation.
- *Refine mesh*: Computing error indicators for the solution, refining and coarsening the mesh, re-partitioning it between processors, and transferring the solution vectors from the previous to the new mesh.

Fig. 4 shows results for these operations, for both weak and strong scaling experiments. From the figures it is apparent that all operations in our program scale well with increasing problem size (weak scaling) once the problem size per MPI process becomes large enough. Likewise, run times can be reduced inversely proportional to the number of processors (strong scaling) as long as the local size or the problem is sufficiently large. The threshold for this scalability is approximately a minimal local problem size of 100,000 degrees of freedom per MPI process, indicated by the vertical lines in Fig. 4. This is also consistent with our observations in [Bangerth et al.(2011)].

We note that in all cases, the time to build the preconditioner and solve the Stokes system dominates all other operations by about an order of magnitude. This is partly due to the fact that, for lack of an alternative, we here start the solver with a zero vector. In contrast, when doing time dependent simulations, we start with the previous solution vector (see the discussion at the end of Section 3.3.2), thereby reducing the fraction of wall time devoted to the Stokes solution from more than 90% to around 70% of the overall run time. With this reduction, we can solve problems at a rate of approximately one time step per minute for large 3d simulations on current cluster hardware when using 100,000 DoFs per processor core, more or less independently of the overall problem size.

4.4 Modeling the earth mantle

To illustrate the ability of ASPECT to solve problems that are relevant to modeling the earth mantle, Fig. 5 and Fig. 6

Table 2. Results for the 2d benchmark problem with uniform mesh refinement. # DoFs indicates the number of degrees of freedom. Reference results from [Blankenbach et al.(1989)].

Mesh size	$\frac{1}{16}$	$\frac{1}{32}$	$\frac{1}{64}$	$\frac{1}{128}$	$\frac{1}{256}$	Reference
# DoFs	5 276	20 532	80 996	$3.2 \cdot 10^5$	$1.3 \cdot 10^6$	—
Period	0.048231	0.048051	0.048031	0.048030	0.048029	0.04803 ± 0.00003
Nu^{\max}	7.4065	7.3822	7.3789	7.3788	7.3788	7.379 ± 0.005
Nu^{\min}	6.5062	6.4717	6.4691	6.4691	6.4692	6.468 ± 0.005
Nu^{\max}	7.2637	7.2047	7.1969	7.1960	7.1960	7.196 ± 0.005
Nu^{\min}	6.7878	6.7949	6.7961	6.7965	6.7966	6.796 ± 0.005
v_{rms}^{\max}	60.726	60.398	60.361	60.359	60.360	60.367 ± 0.015
v_{rms}^{\min}	31.829	31.965	31.981	31.981	31.982	31.981 ± 0.02
v_{rms}^{\max}	58.225	57.517	57.442	57.437	57.436	57.43 ± 0.05
v_{rms}^{\min}	30.392	30.330	30.324	30.323	30.322	30.32 ± 0.03

show snapshots in time of two- and three-dimensional simulations. These simulations use a no-slip velocity boundary condition at the inner rim, a slip boundary condition at the outer rim, and keep the temperature constant at either boundary. Neither computation includes adiabatic heating, but compared to the simple model (1)–(3), the 2d case does include a temperature and pressure (but not strain-rate) dependent viscosity and includes compressibility in the Stokes equation. In both computations, mesh refinement was driven by the second derivative of the gradient which in 3d primarily resolves the inner boundary layer rather than the plumes (however, see also the solution in Section 3.2.1).

These simulations show the excellent spatial resolution adaptive meshes can provide. We will provide results for computations of more direct geodynamic interest in [Geenen et al.(2011)] and elsewhere.

5 CONCLUSIONS AND OUTLOOK

The simulation of convection in the earth mantle is complicated by a host of problems related to the mathematical structure of the equations as well as of the disparity of the lengthscales implied by the sizes of physical coefficients in the earth. Consequently, geodynamics has a long history of the development of methods that can make at least some problems tractable. Nevertheless, fully resolved, three-dimensional simulations have largely remained beyond the ability of current codes and computers.

On the other hand, modern numerical methods can close a significant part of this gap and make many previously intractable problems possible. In this paper, we have presented a collection of state-of-the-art algorithms for mantle convection and their implementation in the ASPECT code. Specifically, we have shown how the interconnected choice of adaptive meshes, discretization, stabilization, solvers and preconditioners leads to a method that not only provides excellent accuracy at very modest numerical cost, but also allows scaling to very large problems with hundreds of millions of unknowns on hundreds or thousands of processor cores with almost perfect complexity. The implementation of these methods is available under an Open Source license in the form of the ASPECT code.

Despite all this, the methods described here are not sufficient to solve entirely realistic models. Specifically, there are at least three obvious places where the simple Boussinesq

model described in equations (1)–(3) is not an adequate description of the real processes that act in the earth interior. First, the various parameters, such as η , ρ , κ or γ , are in reality all nonlinear functions of the solution variables \mathbf{u} , p , T . This dependence can either be direct, such as the dependence of the viscosity on the strain rate, or more indirect by considering which rock phases are thermodynamically stable for the current pressure and temperature value, and then using coefficient values appropriate for this phase. A simple approach to deal with this nonlinearity is to evaluate coefficients at the solution values of the previous time step (or at a value extrapolated from the previous time steps), rendering the system linear again. However, this may lead to an inaccurate account of the transition zones that provide the most direct signal that can be compared with data from seismic inversion. Consequently, an iteration is necessary that resolves the nonlinearity. A common solution is to use a Picard-type iteration (see, for example, [Burstedde et al.(2008)]). A more efficient algorithm may be Newton’s method, but it has to be integrated with the linear solvers and preconditioners to be efficient, and it has to be globalized to guarantee convergence even from poor starting guesses [Nocedal & Wright(1999), Worthen(2012)]. Furthermore, a realistic description of the coefficients often leads to highly heterogeneous coefficients that make the construction of efficient solvers and preconditioners a challenge [Ismail-Zadeh & Tackley(2010), Gerya(2010)].

A second challenge is to deal with compressibility effects. While velocities in the earth mantle are orders of magnitude too slow to compress material based on inertial effects, the large hydrostatic pressure significantly increases the density with depth; temperature and the thermodynamically stable rock phase also affect the density. Consequently, a realistic description needs to modify the continuity equation (2) to read $\nabla \cdot (\rho \mathbf{u}) = 0$ instead, where $\rho = \rho(p, T)$. A simple linearization of this equation in the original set of variables \mathbf{u} , p unfortunately leads to a nonsymmetric variant of the Stokes system for which the choice of preconditioner is entirely unclear; furthermore, it leads to difficult to solve problems with the compatibility condition this equation implies for the right hand side of the divergence equation.

A final topic is that Earth’s mantle is not a homogeneous mixture of materials. Rather, material entrained from plates or the core-mantle boundary may have a significantly different chemical composition. It has also been suggested

Table 3. Results for the 2d benchmark problem with adaptive mesh refinement. The number of degrees of freedom (# DoFs) for each finest mesh size h varies between time steps; the indicated numbers provide a typical range. Reference results from [Blankenbach et al.(1989)].

Finest mesh size # DoFs	$\frac{1}{64}$ 4.5...6.0 · 10 ⁴	$\frac{1}{128}$ 1.6...2.2 · 10 ⁵	$\frac{1}{256}$ 5.6...8.0 · 10 ⁵	Reference —
Period	0.048029	0.048030	0.048030	0.04803 ± 0.00003
Nu ^{max}	7.3809	7.3792	7.3788	7.379 ± 0.005
Nu ^{min}	6.4718	6.4695	6.4691	6.468 ± 0.005
Nu ^{max}	7.1996	7.1967	7.1960	7.196 ± 0.005
Nu ^{min}	6.7986	6.7969	6.7965	6.796 ± 0.005
$v_{\text{rms}}^{\text{max}}$	60.366	60.361	60.360	60.367 ± 0.015
$v_{\text{rms}}^{\text{min}}$	31.980	31.981	31.981	31.981 ± 0.02
$v_{\text{rms}}^{\text{max}}$	57.449	57.434	57.435	57.43 ± 0.05
$v_{\text{rms}}^{\text{min}}$	30.322	30.322	30.322	30.32 ± 0.03

that different layers have different composition [Schubert et al.(2001)]. Simulating heterogeneity entails additional advected fields that describe mass fractions of materials. They can be treated in the same way as the temperature field, with a nonlinear viscosity stabilization of sharp interfaces. Alternatively, a number of approaches such as the particle in cell (PIC) method, marker chains or phase fields have been proposed to avoid smearing of interfaces (for a small sample of methods, see [van Keken & Zhong(1999), Tackley & King(2003), Leng & Zhong(2011), Lin & van Keken(2006)]; see also [Ismail-Zadeh & Tackley(2010), Gerya(2010)] for general overviews).

We are working on extending ASPECT in each of the directions outlined above for future releases.

Acknowledgments. WB would like to thank Scott King for insightful discussions on mantle convection and its simulation.

The first author was supported by the Graduate School in Mathematics and Computation (FMB) at the University of Uppsala, Sweden. The second and third authors are supported in part through the Computational Infrastructure initiative, through the National Science Foundation under Award No. EAR-0949446 and The University of California – Davis. This publication is based in part on work supported by Award No. KUS-C1-016-04, made by King Abdullah University of Science and Technology (KAUST). The third author is also supported in part by an Alfred P. Sloan Research Fellowship.

Some computations for this paper were performed on the “Ranger” and “Lonestar” clusters at the Texas Advanced Computing Center (TACC), and the “Brazos” and “Hurr” clusters at the Institute for Applied Mathematics and Computational Science (IAMCS) at Texas A&M University. Ranger was funded by NSF award OCI-0622780, and we used an allocation obtained under NSF award TG-MCA04N026. The authors acknowledge the Texas A&M Supercomputing Facility for providing computing resources on “Lonestar” useful in conducting the research reported in this paper. Part of Brazos was supported by NSF award DMS-0922866. Hurr is supported by Award No. KUS-C1-016-04 made by King Abdullah University of Science and Technology (KAUST). Some computations were performed on resources provided by SNIC through Uppsala Multidisci-

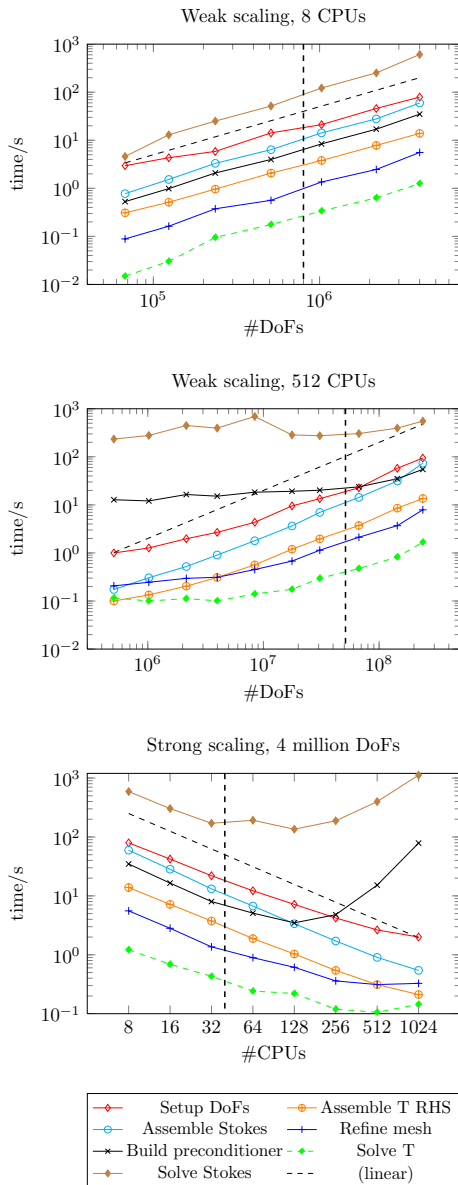
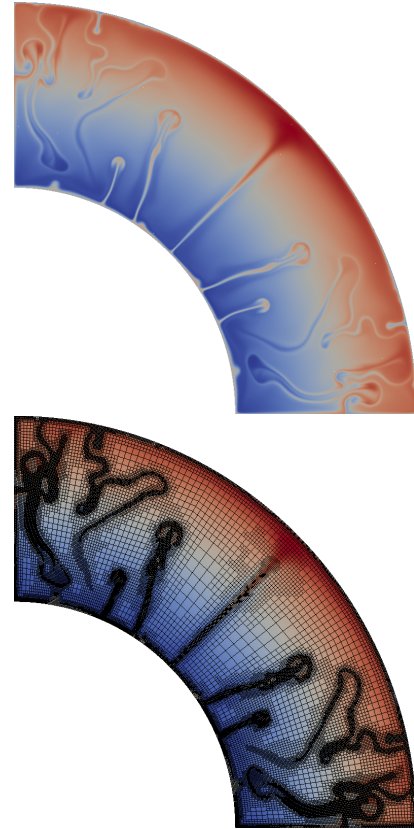
plinary Center for Advanced Computational Science (UPP-MAX) under project p2010002.

REFERENCES

- Ainsworth, M. & Oden, J. T., 2000. *A Posteriori Error Estimation in Finite Element Analysis*, John Wiley and Sons.
- Albers, M., 2000. A local mesh refinement multigrid method for 3-D convection problems with strongly variable viscosity, *J. Comp. Phys.*, **160**, 126–150.
- Babuška, I. & Rheinboldt, W. C., 1978. Error estimates for adaptive finite element computations, *SIAM J. Numer. Anal.*, **15**, 736–754.
- Babuška, I. & Strouboulis, T., 2001. *The Finite Element Method and its Reliability*, Clarendon Press, New York.
- Bangerth, W. & Kanschat, G., 2011. deal.II *Differential Equations Analysis Library, Technical Reference*, <http://www.dealii.org/>.
- Bangerth, W. & Kayser-Herold, O., 2009. Data structures and requirements for hp finite element software, *ACM Trans. Math. Softw.*, **36**(1), 4/1–4/31.
- Bangerth, W. & Rannacher, R., 2003. *Adaptive Finite Element Methods for Differential Equations*, Birkhäuser Verlag.
- Bangerth, W., Hartmann, R., & Kanschat, G., 2007. deal.II – a general purpose object oriented finite element library, *ACM Trans. Math. Softw.*, **33**(4), 24.
- Bangerth, W., Burstedde, C., Heister, T., & Kronbichler, M., 2011. Algorithms and data structures for massively parallel generic adaptive finite element codes, *ACM Trans. Math. Softw.*, **38**(2).
- Bazilevs, Y., Calo, V. M., Tezduyar, T. E., & Hughes, T. J. R., 2007. $YZ\beta$ discontinuity capturing for advection-dominated processes with application to arterial drug delivery, *Int. J. Numer. Meth. Fluids*, **54**, 593–608.
- Blankenbach, B., Busse, F., Christensen, U., Cserepes, L., Gunkel, D., Hansen, U., Harder, H., Jarvis, G., Koch, M., Marquart, G., Moore, D., Olson, P., Schmeling, H., & Schnaubelt, T., 1989. A benchmark comparison for mantle convection codes, *Geophys. J. Int.*, **98**, 23–38.
- Braess, D., 1997. *Finite elements*, Cambridge University Press.
- Brenner, S. C. & Scott, R. L., 2002. *The Mathematical Theory of Finite Elements*, Springer, Berlin-Heidelberg-New York, 2nd edn.
- Brooks, A. & Hughes, T., 1982. Streamline upwind/Petrov-Galerkin formulation for convection dominated flows with particular emphasis on the incompressible Navier-Stokes equations, *Comp. Meth. Appl. Mech. Engrg.*, **32**, 199–259.

Table 4. Selected results for the 3d benchmark problem with uniform mesh refinement. Reference results from [Busse et al.(1993)].

Mesh size	$\frac{1}{24}$	$\frac{1}{32}$	$\frac{1}{48}$	Reference
# DoF	$2.9 \cdot 10^5$	$7.2 \cdot 10^5$	$2.4 \cdot 10^6$	—
Nu	3.5539	3.5447	3.5397	3.5374 ± 0.0005
v_{rms}	40.997	40.999	40.999	40.999 ± 0.004
$T_m(0.75)$	0.52148	0.52148	0.52148	0.52148 ± 0.00003
$u_3(0, 0, 0.5)$	116.605	116.618	116.623	116.625 ± 0.03
$T(0, 0, 0.5)$	0.80126	0.80128	0.80129	0.80130 ± 0.00005
$Q(0, 0)$	6.7679	6.7357	6.7189	6.7127 ± 0.05
$Q(a, b)$	0.7237	0.7205	0.7174	0.7140 ± 0.05

**Figure 4.** Weak and strong scaling experiments for one time step of a 3d mantle convection simulation. In each of the graphs, the vertical line indicates 10^5 degrees of freedom per processor core; cores have more than than this threshold to the right of the line in the top two panels, and to the left of the line in the strong scaling results.**Figure 5.** Solution of a 2d convection problem on a quarter shell domain. The solution has around 700,000 degrees of freedom and was obtained on 16 processors; each time step took less than one second on average. Top: Temperature field. Bottom: Adaptive mesh of the same solution.

- Burstedde, C., Ghattas, O., Gurnis, M., Tan, E., Tu, T., Stadler, G., Wilcox, L. C., & Zhong, S., 2008. Scalable adaptive mantle convection simulation on petascale supercomputers, in *SC '08: Proceedings of the International Conference for High Performance Computing, Networking, Storage, and Analysis*, ACM/IEEE.
- Burstedde, C., Burtscher, M., Ghattas, O., Stadler, G., Tu, T., & Wilcox, L. C., 2009. ALPS: A framework for parallel adaptive PDE solution, *J. Physics: Conf. Series*, **180**, 012009.
- Burstedde, C., Wilcox, L. C., & Ghattas, O., 2011. **p4est**: Scalable algorithms for parallel adaptive mesh refinement on forests of octrees, *SIAM J. Sci. Comput.*, **33**(3), 1103–1133.
- Busse, F., Christensen, U., Clever, R., Cserepes, L., Gable, C., Giannandrea, E., Guillou, L., Houseman, G., Nataf, H.-C.,

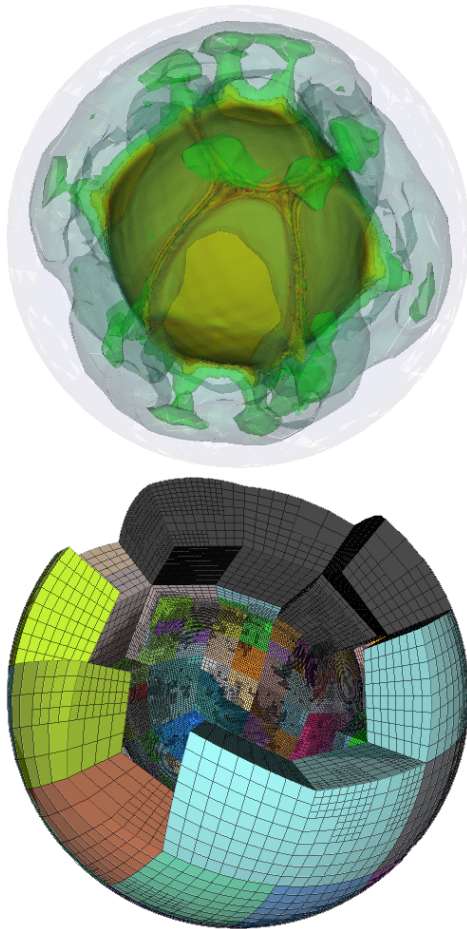


Figure 6. Solution of a 3d convection problem in a spherical shell. Top: Isocontours of the temperature field. Bottom: Partitioning of the domain onto 512 processors. The subdomains and corresponding meshes of the first half of all processors are shown. The mesh has 1,424,176 cells, and the solution has approximately 54 million unknowns (39 million velocities, 1.7 million pressures, and 13 million temperatures).

- Ogawa, M., Parmentier, M., Sotin, C., & Travis, B., 1993. 3D convection at infinite Prandtl numbers in cartesian geometry — a benchmark comparison, *Geophys. Astrophys. Fluid Dynamics*, **75**, 39–59.
- Carey, G. F., 1997. *Computational Grids: Generation, Adaptation and Solution Strategies*, Taylor & Francis.
- Chen, Z., 2006. *Computational Methods for Multi-phase Flows in Porous Media*, SIAM.
- Davies, D. R., Davies, J. H., Hassan, O., Morgan, K., & Nithiarasu, P., 2007a. Investigations into the applicability of adaptive finite element methods to two-dimensional infinite Prandtl number thermal and thermochemical convection, *Geoch. Geophys. Geosystems*, **8**, Q05010/1–25.
- Davies, D. R., Davies, J. H., Hassan, O., Morgan, K., & Nithiarasu, P., 2007b. Adaptive finite element methods in geodynamics: Convection dominated mid-ocean ridge and subduction zone simulations, *Int. J. Numer. Meth. Heat Fluid Flow*, **18**, 1015–1035.
- Donea, J. & Huerta, A., 2003. *Finite Element Methods for Flow Problems*, J. Wiley & Sons, Chichester.
- Elman, H., Silvester, D., & Wathen, A., 2005. *Finite Elements and Fast Iterative Solvers with Applications in Incompressible Fluid Dynamics*, Oxford Science Publications, Oxford.
- Gago, J. P. d. S. R., Kelly, D. W., Zienkiewicz, O. C., & Babuška, I., 1983. A posteriori error analysis and adaptive processes in the finite element method: Part II — Adaptive mesh refinement, *Int. J. Num. Meth. Engrg.*, **19**, 1621–1656.
- Gee, M. W., Siefert, C. M., Hu, J. J., Tuminaro, R. S., & Sala, M. G., 2006. ML 5.0 Smoothed Aggregation User's Guide, Tech. Rep. 2006-2649, Sandia National Laboratories.
- Geenen, T., ur Rehman, M., MacLachlan, S. P., Segal, G., Vuik, C., van den Berg, A. P., & Spakman, W., 2009. Scalable robust solvers for unstructured FE geodynamic modeling applications: Solving the Stokes equation for models with large localized viscosity contrasts, *Geochem. Geophys. Geosyst.*, **10**(9), Q09002.
- Geenen, T., Heister, T., Kronbichler, M., & Bangerth, W., 2011. 3d high resolution phase distribution and seismic velocity structure evolution of the transition zone: modeled in a full spherical-shell compressible mantle convection context, *in preparation*.
- Gerya, T., 2010. *Introduction to Numerical Geodynamic Modelling*, Cambridge University Press.
- Girault, V. & Raviart, P.-A., 1986. *Finite Element Methods for the Navier–Stokes Equations*, Springer–Verlag, New York.
- Guermond, J.-L., Pasquetti, R., & Popov, B., 2011. Entropy viscosity method for nonlinear conservation laws, *J. Comput. Phys.*, **230**, 4248–4267.
- Hackbusch, W., 1985. *Multi-grid Methods and Applications*, Springer.
- Hairer, E. & Wanner, G., 1991. *Solving Ordinary Differential Equations II. Stiff and Differential-Algebraic Problems*, Springer-Verlag, Berlin.
- Heroux, M. A. et al., 2011. Trilinos web page, <http://trilinos.sandia.gov>.
- Heroux, M. A., Bartlett, R. A., Howle, V. E., Hoekstra, R. J., Hu, J. J., Kolda, T. G., Lehoucq, R. B., Long, K. R., Pawlowski, R. P., Phipps, E. T., Salinger, A. G., Thornquist, H. K., Tuminaro, R. S., Willenbring, J. M., Williams, A., & Stanley, K. S., 2005. An overview of the Trilinos project, *ACM Trans. Math. Softw.*, **31**, 397–423.
- Ismail-Zadeh, A. & Tackley, P., 2010. *Computational Methods for Geodynamics*, Cambridge University Press.
- Kameyama, M., 2005. ACuTEMan: A multigrid-based mantle convection simulation code and its optimization to the Earth simulator, *J. Earth Simulator*, **4**, 2–10.
- King, S. D., Raefsky, A., & Hager, B. H., 1990. Conman: Vectorizing a finite element code for incompressible two-dimensional convection in the earth's mantle, *Phys. Erath Planet. Inter.*, **59**, 195–207.
- Kronbichler, M. & Bangerth, W., 2011. deal.II tutorial program step-31, http://www.dealii.org/developer/doxygen/deal.II/step_31.html.
- Kronbichler, M., Heister, T., & Bangerth, W., 2011. deal.II tutorial program step-32, http://www.dealii.org/developer/doxygen/deal.II/step_32.html.
- Leng, W. & Zhong, S., 2011. Implementation and application of adaptive mesh refinement for thermochemical mantle convection studies, *Geoch. Geoph. Geosystems*, **12**, Q04006.
- LeVeque, R. J., 2002. *Finite Volume Methods for Hyperbolic Problems*, Cambridge Texts in Applied Mathematics, Cambridge.
- Lin, S.-C. & van Keken, P. E., 2006. Deformation, stirring and material transport in thermochemical plumes, *Geoph. Res. Letters*, **33**, L20306/1–5.
- Moresi, L., Zhong, S. J., & Gurnis, M., 1996. The accuracy of finite element solutions of Stokes' flow with strongly varying viscosity, *Phys. Erath Planet. Inter.*, **97**, 83–94.
- Nocedal, J. & Wright, S. J., 1999. *Numerical Optimization*, Springer Series in Operations Research, Springer, New York.
- Quarteroni, A. & Valli, A., 1994. *Numerical Approximation of*

- Partial Differential Equations*, Springer, Heidelberg.
- Saad, Y., 2003. *Iterative Methods for Sparse Linear Systems*, SIAM, Philadelphia, 2nd edn.
- Schubert, G., Turcotte, D. L., & Olson, P., 2001. *Mantle Convection in the Earth and Planets, Part 1*, Cambridge.
- Sheldon, J. W., Zondek, B., & Cardwell, W. T., 1959. One-dimensional, incompressible, non-capillary, two-phase fluid flow in a porous medium, *Trans. SPE AIME*, **216**, 290–296.
- Silvester, D. & Wathen, A., 1994. Fast iterative solution of stabilised Stokes systems. Part II: Using general block preconditioners, *SIAM J. Numer. Anal.*, **31**, 1352–1367.
- Stadler, G., Gurnis, M., Burstedde, C., Wilcox, L. C., Alisic, L., & Ghattas, O., 2010. The dynamics of plate tectonics and mantle flow: From local to global scales, *Science*, **329**, 1033–1038.
- Stone, H. L. & Garder, A. O., 1961. Analysis of gas-cap or dissolved-gas reservoirs, *Trans. SPE AIME*, **222**, 92–104.
- Tackley, P. J. & King, S. D., 2003. Testing the tracer ratio method for modeling active compositional fields in mantle convection simulations, *Geoch. Geoph. Geosystems*, **4**, 2001GC000214/1–15.
- Tan, E. & Gurnis, M., 2007. Compressible thermochemical convection and application to lower mantle structures, *J. Geophys. Res.*, **112**.
- Trottenberg, U., Oosterlee, C., & Schüller, A., 2001. *Multigrid*, Elsevier Academic Press, London.
- Tuminaro, R. & Tong, C., 2000. Parallel smoothed aggregation multigrid: aggregation strategies on massively parallel machines, in *Super Computing 2000 Proceedings*.
- van Keken, P. & Zhong, S., 1999. Mixing in a 3D spherical model of present-day mantle convection, *Earth Planet. Science L.*, **171**, 533–547.
- Worthen, J., 2012. *Inverse Problems in Mantle Convection: Models, Algorithms, and Applications*, Ph.D. thesis, University of Texas at Austin, in preparation.
- Zhong, S., McNamara, A., Tan, E., Moresi, L., & Gurnis, M., 2008. A benchmark study on mantle convection in a 3-D spherical shell using CitcomS, *Geochem. Geophys. Geosyst.*, **9**, Q10017.